A New Contact Time Model for the Mechanistic Assessment of Local Heat Transfer Coefficients in Bubble Column Using Both the Four-Optical Fiber Probe and the Fast Heat Transfer Probe-Simultaneously

Moses Kagumba, Hayder Al-Naseri, Muthanna H. Al-Dahhan

PII: S1385-8947(18)32518-X
DOI: https://doi.org/10.1016/j.cej.2018.12.046
Reference: CEJ 20586

To appear in: *Chemical Engineering Journal*

Received Date: 28 June 2018
Revised Date: 6 December 2018
Accepted Date: 7 December 2018

Please cite this article as: M. Kagumba, H. Al-Naseri, M.H. Al-Dahhan, A New Contact Time Model for the Mechanistic Assessment of Local Heat Transfer Coefficients in Bubble Column Using Both the Four-Optical Fiber Probe and the Fast Heat Transfer Probe-Simultaneously, *Chemical Engineering Journal* (2018), doi: https://doi.org/10.1016/j.cej.2018.12.046

A New Contact Time Model for the Mechanistic Assessment of Local Heat Transfer Coefficients in Bubble Column Using Both the Four-Optical Fiber Probe and the Fast Heat Transfer Probe-Simultaneously

Moses Kagumba[¥], Hayder Al-Naseri[†€], and Muthanna H. Al-Dahhan[††*♣]

[†]Chemical and Biochemical Engineering Department

[*]Mining and Nuclear Engineering Department

Missouri University of Science and Technology, Rolla, MO 65409, USA

[♣]Cihan University-Erbil, Iraq

[€]Chemical Engineering Department, Tikrit University, Tikrit-IRAQ

[¥] Currently at The Department of Chemical and Petroleum Engineering, The Technical University of Kenya, Nairobi, City-Square 52428 – 00200. KENYA

Abstract

The purpose of this study is to analytically assess the local heat transfer coefficients by using the local bubble properties, which include the local gas holdup, bubble pass frequency, bubble chord length, and axial bubble velocity in a bubble column reactor. Therefore, for the first time, a combined probe that consists of a fast-response heat transfer coefficients probe and an advanced four-point optical probe was used for simultaneously measuring the heat transfer coefficients and the bubble properties, respectively. A new model, which has been developed, applied to estimate the contact time (τ) between the thin liquid film on the heating surface and the bulk liquid, which is one of the two parameters required in the mechanistic equation for determining the heat transfer coefficients. The experiments were conducted using a Plexiglas bubble column of 0.44 m diameter and 3.66 m height. Analytically, the consecutive film and the renewal mechanistic model of the unsteady-state surface have been used to calculate the rate and coefficients of the heat transfer. Results illustrate that the heat transfer coefficients is significantly affected by the local bubble properties and their distributions over the surface of the heat sensor. However, the contact time (τ) is a function for the local gas holdup and the bubble pass frequency. Thus, the variation in the local heat transfer coefficients with the contact time is due to the bubble pass frequency and the local gas holdup. A very good agreement, within 13 %, was found between the predicted and the experimental values of the heat transfer coefficients, even though the model overpredicts the heat transfer coefficients at all the evaluated conditions.

Keywords: Bubble columns, Bubble dynamics, Heat transfer coefficients, Fischer-Tropsch Synthesis.

† Corresponding author at Chemical & Biochemical Engineering Department, Missouri University of Science and Technology, Rolla, MO, 65409. Tel.: +1 573-578-8973. E-mail: aldahhanm@mst.edu

1. Introduction

Among the outstanding characteristics of bubble and slurry bubble column reactors that make them desirable is the high rate of heat transfer and mass transfer due to strong mixing and phase interactions. A number of industrial processes carried out in bubble and slurry bubble columns are characterized by high exothermic reactions. For instance, the Fischer-Tropsch synthesis is a highly exothermic process with a heat of reaction in the region of -172 kJ/mol of CO converted [1]. Therefore, proper design for the heat removal surfaces is essential to keep the reactor at the design temperature, which in turn maintains the reaction's integrity, catalyst activity, and product quality in bubble and slurry bubble columns.

The prediction of the heat transfer rate and heat transfer coefficients has been addressed in numerous studies that were conducted in two-phase and three-phase systems, and several correlations have been proposed [2], [3], [12–15], [4–11]. However, these studies have developed the correlations according to experimental results for the heat transfer and bubble dynamics, which were conducted separately. Thus, the heat transfer studies have been achieved separately from the bubble dynamics studies under different operating conditions and a different scale setup. Wu [16] studied bubble dynamics and heat transfer separately in bubble columns. It can be deduced from his work that the heat transfer rate increases with bubble size, bubble velocity, and bubble pass frequency. Kumar et al. [17] investigated the effect of bubble pass on the instantaneous heat transfer rate in gas-liquid and gas-liquid-solid systems. They revealed that when a single bubble is injected into liquid or liquid-solid systems, the heat transfer rate through the bubble wake is enhanced. They found that in the wake region, which is located a distance behind the bubble and is enhanced by increasing the bubble size, the maximum heat transfer occurs in the upward flow. The effect of a large population of bubbles,

which is characteristic of the real system of industrial interest remains mostly unreported. Furthermore, studies conducted by Kagumba and Al-Dahhan [18] and Kagumba [19] together with the critical reviews [16], [17], and [19] point at a close relation among the bubble properties and the heat transfer rate in two-phase and three-phase systems in general and bubble and slurry bubble columns in particular.

In this study, the mechanistic approach of Wasan and Ahluwalia [21] has been implemented to explain the interrelation between the measured heat transfer coefficients and bubble dynamics and to predict the heat transfer coefficients mechanistically without using fitted parameters. A new model related to the contact time needed for the mechanistic approach has been developed based on the bubble dynamics measured by a sophisticated 4-point fiber optical probe, which include the local gas holdup, bubble pass frequency, bubble chord length, and bubble axial velocity. The mechanistic analysis has been compared with measured heat transfer coefficients using a non-invasive advanced heat transfer probe.

1.1. Reported Mechanism of Heat Transfer

Bubbles in gas-liquid and gas-liquid-solid systems induce the turbulence and mixing that in turn significantly enhances the heat and mass transfer. Thus, the high heat transfer rate in the bubble and slurry bubble column reactors is attributed mainly to bubble-induced turbulence [17], [22]. Based on the experimental and theoretical studies, the heat exchange between a flowing fluid that is adjacent to the surface and the heat transfer surface has been governed by the theory of a film series and renewal surface [19], [21–23].

The film theory was first proposed by Nernst [24]. It has been applied to both heat and mass transfer with some success. According to this theory, heat transferred across a unit area of the

interface per unit time is assumed to be proportional to the temperature gradient between the bulk fluid and the interface that would give the heat flux, q and the heat transfer coefficients, h, which equals (k/δ). This model indicates a linear relationship between the thermal diffusivity and the heat flux. This model oversimplifies the actual conditions near a phase boundary. Furthermore, the concept of the theory supposes that a stagnant film of a definite but unknown thickness exists. Therefore, according to Azbel [25], this theory's main weakness is the introduction of a uniform film of thickness, δ_e. According to Fick's second law of unsteady-state diffusion, Ralph and Higbie [26] suggested a penetration theory where mass and heat transfer are observed as an unsteady-state process, where the film theory has not considered the unsteady-state phenomenon by assuming that the phenomena of heat and mass transfer occur during the repeated contact of the gas-solid with the interface of liquid. Therefore, renewal of the liquid elements continually replaces those interacting with the interface. Based on that, at each contact period between the liquid element and the interface, the gradient in concentration or temperature will be increased, and hence, mass or heat is transferred to the new element. According to that, the contact time between the interface and small eddies is short. Therefore, interpreting the heat and mass transfer phenomena by unsteady-state characteristics will be more reasonable to this model. Besides, all the eddies are assumed to stay in contact with the interface for same length of time (θ), during which diffusion of matter (heat and mass) occurs into the eddy, which for heat can be described by a one-dimension system equation [26]. Danckwerts [27] modified the penetration theory [26] and came up with the surface renewal model in order to account for the different times of contact by different eddies that have different sizes. Thus, the fluid elements can have a surface residence time ranging from zero to infinity. Hence, the average heat transfer coefficients is shown in equation (1):

$$h_w = \sqrt{(\alpha s)\ \rho\ C_p} \quad (1)$$

where s is the fractional rate of surface renewal by the elements, a parameter which is not easy to determine experimentally or theoretically.

Research conducted to study the characteristics of the liquid film both experimentally and theoretically, suggests that a thin film lies between a solid surface and the flowing fluid over the solid surface [28]–[30]. Thus, predicting the heat transfer coefficients using the film theory alone is not appropriate due to its shortcoming that was stated earlier. However, using the penetration theory alone would not be sufficient, since different eddies have a different distribution in the contact time. The surface renewal model would be more appropriate, but on its own, the presence of the stagnant liquid film would not be accounted for. Thus, combining both the surface renewal model and the film theory is the most appropriate mechanism for estimating the heat transfer rate.

Accordingly, Wasan and Ahluwalia [21] developed a mechanistic model to predict the heat transfer coefficients based on a mechanism where heat transfer enhancement due to bubble pass was expressed in terms of film theory and the unsteady-state consecutive surface renewal model (also known as the modified penetration theory). Such a mechanism suggests that there is a thin film of uniform thickness, δ, lying parallel to and covering the heat transfer surface. Due to the bubble motion around the film, a liquid element is moved to the outer surface of the film from the bulk. In this case, heat is transferred to the element by unsteady-state conduction during the contact period and then washed away. A short time later, another fluid element is moved to the same surface and the process repeats. Figure 1 illustrates the consecutive film and unsteady-state surface renewal heat transfer mechanism from the heating source into the bulk fluid.

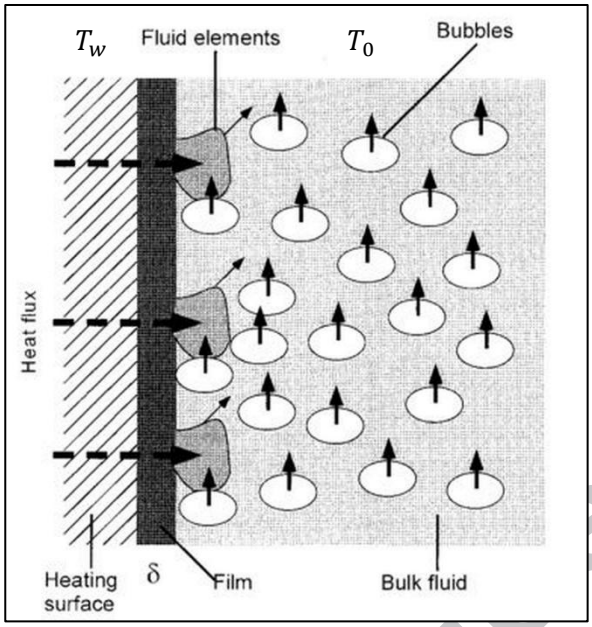

Figure 1. Consecutive film and unsteady-state surface renewal mechanism modified from Wasan and Ahluwalia (1969)

This proposed approach differs from the concepts of the combination of film-penetration theory, where the latter recommended film theory for long contact times and penetration theory for short contact times. In the approach of Wasan and Ahluwalia [21], a uniform film (thinner than would be predicted by film theory alone) that can be estimated by Prandtl's boundary-layer theory is regarded to lie adjacent to the heat transfer surface, and a mass of fluid exchanges heat by unsteady-state conduction at the outer edge of such film. Hence, there is a dynamic change of the temperature of the interface between the film and the fluid element. According to this approach, Wasan and Ahluwalia [21] developed a mechanistic model to predict the heat transfer coefficients from the heat exchanging surface to flowing gas-liquid and gas-liquid-solid mediums as outlined below.

In such an approach, the temperature of the fresh fluid element coming from the bulk to the outer surface of the film is assumed uniform and equal to the bulk fluid temperature, $T_{y=0}$ at

time$(t) = 0$. By assuming no energy storage in the film, the instantaneous heat transfer rate to the fluid mass was given as shown in equation (2):

$$q = -k\left(\frac{\partial T}{\partial Y}\right)_{y=0} = h\left(T_w - T_{y=0}\right) \tag{2}$$

where y is the distance within the fluid mass measured from the edge of the film, and the film maintains a uniform film thickness of δ, and the heat transfer coefficients is $h = k/\delta$. This begins with the two-dimensional unsteady-state equation for heat conduction to the fluid mass, as shown in equation (3):

$$\frac{\partial T}{\partial t} = \alpha\left(\frac{\partial^2 T}{\partial y^2} + \frac{\partial^2 T}{\partial z^2}\right) \tag{3}$$

Wasan and Ahluwalia [21] mechanistically obtained the equation (4) for the heat transfer coefficients:

$$h_w = \frac{2k}{\sqrt{\pi \alpha t_c}} - \frac{k\delta}{\alpha t_c}\left[1 - e^{\frac{\alpha t_c}{\delta^2}}\, refc\frac{\sqrt{\alpha t_c}}{\delta}\right] \tag{4}$$

Equation (4) can be used for modeling the instantaneous and the average heat transfer coefficients, h_w, which depends upon the film thickness, δ, contact time, t_c, and the physical properties, k and α. The model equation (4) has been used to predict the heat transfer coefficients in two-phase and three-phase flow systems [17], [22], [23], [31]. It can give the local heat transfer coefficients $h(r)$ by locally having different estimated values of t_c and δ. The needed film thickness, δ, and the contact time, t_c, have been estimated by different investigators using the few available empirical correlations as highlighted in section 1.2 and 1.3, which includes the shortcomings associated with the current model or equation used to estimate the contact time t_c.

1.2. Film Thickness Estimation

One of the two needed parameters in the mechanistic equation (4) is the film thickness, (δ). The film thickness accounts for the heat transfer resistance. In this work, the model of Azbel [25] for the border diffusion layer has been used, which was modified by Kumar and Fan [32] and Yang et al. [22] to predict the film thickness, δ. According to this model, the distribution of the diffusing matter (mass or heat) in a turbulent stream has a four-layer structure. Namely, the diffusion sublayer δ, which is also known as the thermal boundary layer and is in contact with the solid interface, is followed by the laminar viscous sublayer δ_0, then the turbulent boundary layer, and finally the main turbulent stream. According to Azbel [25], the relation between the diffusion sublayer and the viscous sublayer is shown in equation (5):

$$\delta = \left(\frac{\alpha}{\nu}\right)^{1/n} \delta_0 \tag{5}$$

where ν is the kinematic viscosity, and α is the thermal diffusivity. According to the experimental data for liquid-solid interface flows, it has been found [25] that $n \cong 3$. The thickness of the laminar viscous sublayer, δ_0, can be estimated by solving Prandtl's boundary-layer equations [33] as shown in Equations (6-7):

$$\frac{\partial u}{\partial t} + u\frac{\partial u}{\partial x} + v\frac{\partial u}{\partial y} = -\frac{1}{\rho}\frac{\partial p}{\partial x} + \nu\frac{\partial^2 u}{\partial y^2} \tag{6}$$

$$\frac{\partial u}{\partial x} + \frac{\partial v}{\partial y} = 0 \tag{7}$$

with the boundary conditions as shown:

$$y = 0: \quad u = v = 0$$

$$y = \infty: \quad u = U(x,t)$$

where $U(x,t)$ is considered a known unsteady-state potential flow to determine the pressure distribution, according to Schlichting [34]. Thus, using the square dimensions of the heat flux sensor utilized in this work as (L = 0.011 m) leads to the thickness of the laminar sublayer as shown in equation (8):

$$\delta_0 = \frac{8.68L}{Re^{3/4}} \tag{8}$$

Hence, the film thickness is also known as the thermal boundary layer, δ, which can be estimated by combining equations (5) and (8) to give equation (9) [22], [23], [25]:

$$\delta = \frac{8.68L}{Re^{3/4}Pr^{1/3}} \tag{9}$$

where $R_e, and\ Pr$ are Reynold number $(U_b L\rho_l/\mu_l)$, and Prandtl number $\left(C_{pl}\mu_l/K_l\right)$, respectively.

1.3. Reported Contact Time Estimation

Due to the limitation of the measurements and the unavailability of techniques, only a few models for the estimation of the contact time between the liquid elements and the thin film have been proposed. Kumar and Fan [32] assume that the absolute bubble rise velocity can be taken as an estimate of the characteristic velocity of a fluid element near the heat transfer surface. They obtained the absolute bubble rise velocity by following each bubble, frame by frame, in the video recording over a certain distance. Therefore, during the heat transfer enhancement by the bubble wake, the time available for heating by conduction before each fluid element passes the heat transfer surface may be approximated. They assumed that all the fluid elements renew the probe surface at the same rate, and hence there is no distribution of residence time, which is in line with the penetration theory [26]. Thus, they proposed equation (10) to estimate the

contact time, t_c, in gas-liquid (bubble columns) and gas-liquid-solid (slurry bubble columns) systems:

$$t_c = \frac{L}{U_b} \tag{10}$$

where L is the vertical length of the heat flux sensor and U_b is the bubble rise velocity. During this time, unsteady heat conduction occurs and starts at a distance from the heat transfer surface, which is equivalent to the thickness of the thin film. One of the main drawbacks of this approach is that the video can only be used for transparent mediums and at very low superficial gas velocity, which minimizes its applicability in systems requiring higher gas velocities.

Yang et al. [22] alongside Kumar and Fan [32] assumed that the contact time is equal to the contact time between the bubbles and the film and used the same equation proposed by the latter (equation 10). While using a cylindrical rod-type of the heat transfer probe, Li and Prakash [33] assumed that the contact time, θ_c can be modeled as shown in equation (11):

$$\theta_c = \frac{d_p}{U_{b,L}} \tag{11}$$

where d_p is the diameter of the cylindrical probe, used horizontally, while $U_{b,L,}$ is the rise velocity of large bubbles. These approaches only provided single values for the contact time to obtain the single averaged value of the heat transfer coefficients using the mechanistic model of equation (4). However, in the multiphase flow systems, particularly bubble and slurry bubble columns, populations of bubbles and their properties (velocity, size, pass frequency, specific interfacial area, local gas hold-up) exist at a particular superficial gas velocity [18], [19], [35], [36]. Theoretically, with a reasonable measurement approach, the distribution in the contact time can be obtained from the above models shown in equation (11) [19]. Furthermore, as will

be demonstrated in section 3.1, the contact time estimated by equations (10) and (11) reaches a plateau as the superficial gas velocity increases in the deep churn turbulent flow regime, which is not the proper trend representing the nature of the turbulent flow regime. Therefore, a mechanistic model needs to be developed that properly describes the trend of the contact time with superficial gas velocity in the churn turbulent flow regime.

2. Experimental Work

2.1. Experimental Set-Up

The schematic of the column used and the general features of the experimental system are shown in Figure 2. In order to illustrate the heat transfer in a mechanistic manner based on the discussed model above, simultaneous measurements of both the heat transfer coefficients and bubble dynamics were conducted in a large-scale bubble column consisting of a 0.44 m inside diameter and 3.66 m height. In all the experiments, the dynamic bed height has been maintained constant at a level of 2.67 m (z/D = 6.0) above the gas distributor by adjusting the amount of liquid loaded in the column. Filtered oil-free dry air was used as the gas phase while, filtered soft water was used as the liquid phase. The superficial gas velocity varied up to 0.45 m/s, covering partly transition and mainly the churn turbulent flow regimes. The compressed filtered oil-free dry air was introduced continuously from the bottom of the column.

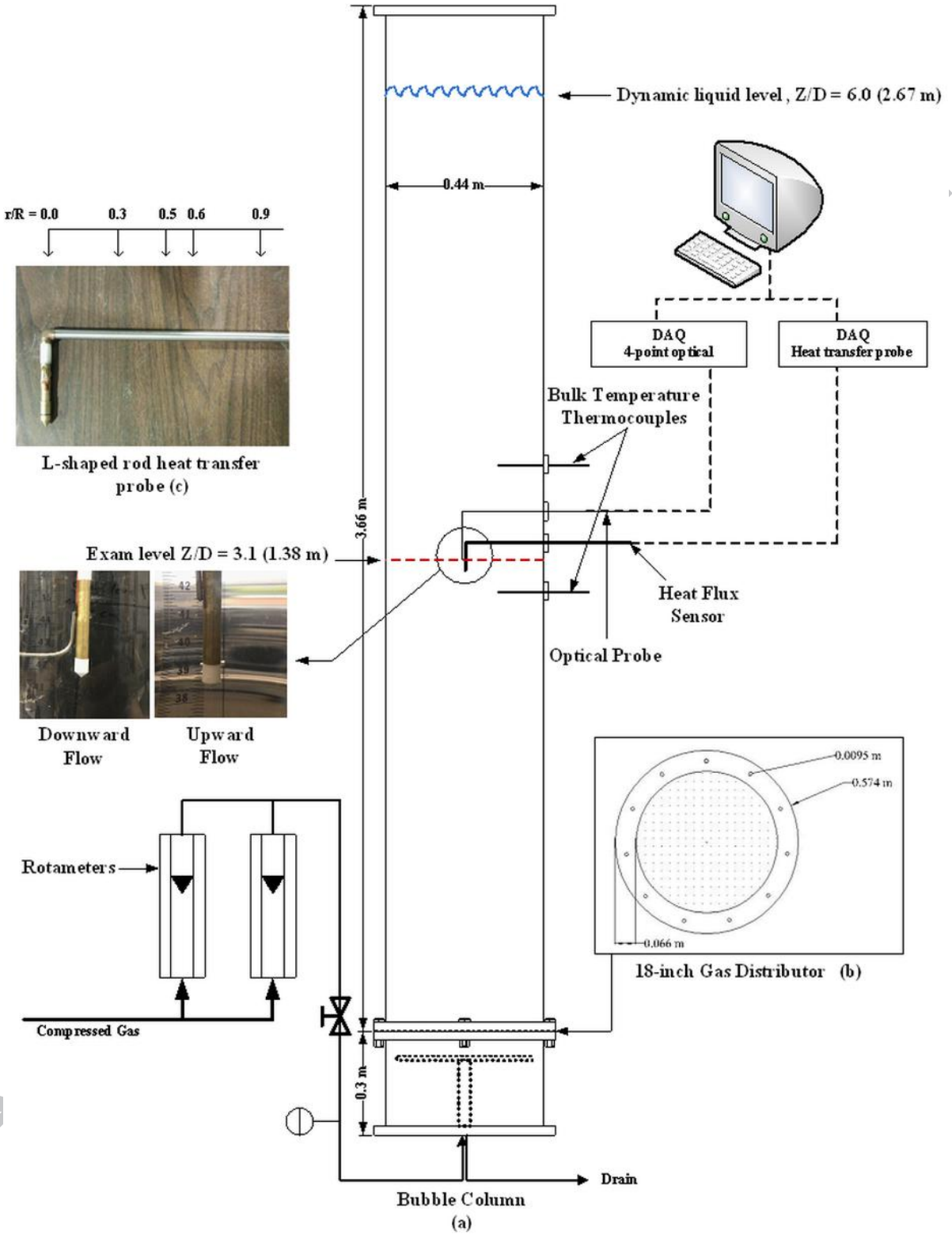

Figure 2. Schematic diagram of the experimental system; a. Bubble column b. Gas distributor c. L-shaped rod heat transfer probed. Both heat transfer and 4-point optical probe

2.2. Measurements Techniques

In this study, two measurement techniques have been used to measure the heat transfer coefficients and the bubble dynamics simultaneously. Both measurements have been achieved by using a hybrid probe that consists of two independently fabricated probes, namely the advanced four-point fiber optical probe and a fast response heat transfer probe. The advanced four-point fiber optical probe has been used to measure the bubble properties which include local gas hold up, bubble pass frequency, axial bubble velocity (upward and downward), and the specific interfacial area, as well as the bubble chord lengths that are characteristic of bubble sizes.

Further, the probe's tips would affect surrounding turbulence which would introduce bubble pass frequency. However, this would be insignificant in the intense churn turbulent flow regime. The non-invasive fast response heat transfer probe has been used to measure the heat flux from which the heat transfer coefficients can be estimated. Figure 3 illustrates the four-point optical probe that is utilized in this work, initially developed by Frijlink [37] at the Kramers laboratory in the Department of Multiscale Physics at the Technical University of Delft in the Netherlands. Subsequently, Xue [38] and Xue et al. [39] have developed and validated a new data processing algorithm for two-phase system, which later, was validated in three-phase systems by Wu [16]. In addition, Youssef and Al-Dahhan [36], and Youssef [40] applied the four-point optical probe in bubble columns equipped with a dense internal structure. Most recently, Kagumba [19] further validated the four-point optical probe in gas-liquid and gas-liquid-solid systems with and without dense internals. Therefore, the same sampling time and frequency of 138 (sec) and 40 kHz, respectively, have been used in this study. However,

more detailed information about probe construction and principle working are available in [18], [19], [39].

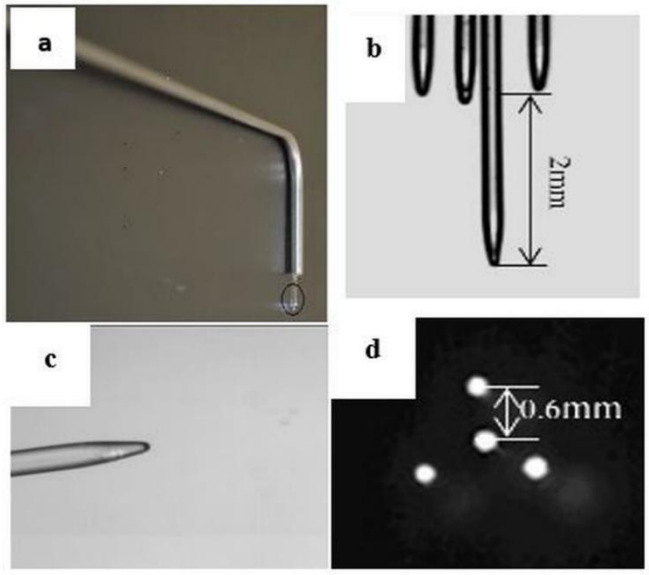

Figure 3. Configurations of the four-point optical probe (a) Optical probe tips (b) Side view of the four-point probe tip (c) TEM image of the finished tip, (d) Top view of four points probe tips

The other probe is a fast-response heat transfer coefficients probe (L-shaped type) as shown in Figure 2 c, a modified version of the heat transfer probe initially proposed by Li and Prakash [31]. The instantaneous heat flux was measured by utilizing a micro-foil heat flux sensor (11 mm × 11 mm × 0.08 mm) from RdF Corporation (No. 20453-1). The micro-foil heat flux sensor was flush-mounted on the outer surface of a hollow brass cylinder to make the measurement a non-invasive one. The micro-foil sensor has both the heat flux sensor and the micro-thermocouple. Thus, the micro-foil sensor can simultaneously measure both the local instantaneous heat flux from the probe to the bulk fluid and the instantaneous surface temperature of the probe. A small cylindrical cartridge heater (Chromalox, model number CIR-1012) was installed inside the hollow brass cylinder. The AC power that is supplied to the cartridge heater was varied to regulate the supplied power in the range of 0 to 50 V. To

complete the heat transfer probe assembly, the tube and fittings were separated by Teflon, which reduces the heat loss transferred from the heater to the connections. Two additional T-type thermocouples were installed in the column to measure the bulk fluid temperature. The measured signals of the heat flux, in the range of microvolts, need to be amplified before being sent to the data acquisition (DAQ) system. Abdulmohsin and Al-Dahhan [41] investigated the effect of the presence of internals on the heat transfer coefficients in bubble column reactor of a 0.19 m inside diameter and 2 m height, using the fast heat transfer probe technique. An air-water system was utilized with superficial gas velocity varying from U_g= 0.03 to 0.2 m/s. They collected the measurement data of heat transfer coefficients with sampling at 50 Hz and 40 seconds of sampling time. Accordingly, in this work, the heat flux signals after was amplified together with the signals from the thermocouples were sampled at 50 Hz. While, the sampling time of collection data was tested by drawing the heat transfer coefficients as a function for different sampling times as shown in Figure 4. Therefore, Figure 4 revealed that no significant variation for the heat transfer coefficients after sampling time = 45 seconds. Hence, all measurements were conducted with sampling time = 90 seconds. Since this work studied the local time-averaged heat transfer coefficients in the fully developed region, the thermocouples were installed close to the heat transfer probe, about 0.1 m. in axial distance both above and below the probe. Is worth to mention, the experiment started to collect the heat transfer coefficients measurements after the difference between the temperature of bulk and the temperature of probe surface reached a steady state, which indicates that the thermal and the hydrodynamics properties being stable in the bubble column reactor. Furthermore, data obtained for the heat transfer coefficients, and the bubble dynamics have been exhibited in this work with the error bar, which represents the three replications of

measurements. However, more information about the procedure of the experimental method that relates to the fast heat transfer coefficients and the four-point optical probe is available in Kagumba and Al-dahhan [18], and Kagumba [19].

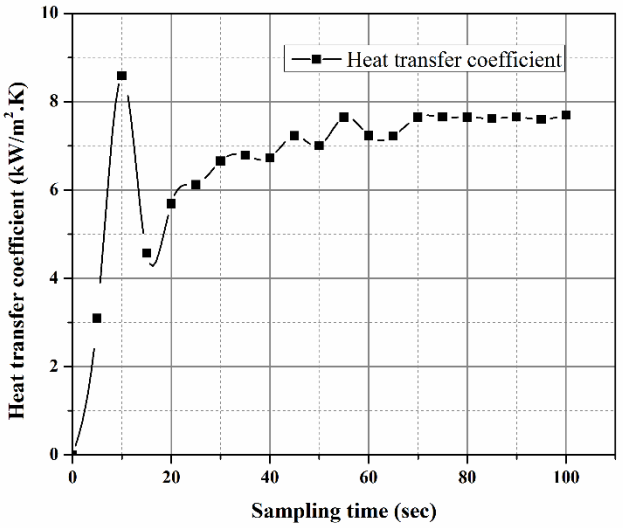

Figure 4. The stability of heat transfer coefficients with sampling time of the collecting data

Figure 5 shows the schematic of the heat transfer probe. The averaged values of the temperatures obtained by these thermocouples were representative of and used as the bulk temperature. Both probes (consisting of the heat transfer probe and the four-point optical probe) were mounted in the fully developed flow region at level Z = 1.38 m (i.e., Z/D = 3.1) of the columns for all the measurements, and this level above the gas distributor was chosen since it represents a fully developed flow region where the bubble properties remain nearly unchanged, with the optical probe mounted just off the surface of the heat flux sensor. Only one axial location, in the fully developed flow region, was used for all the measurements since there is a negligible variation on the bubble properties within this flow region [38]. Both probes were

fabricated in the Multiphase Flow and Multiphase Reactor Engineering and Application Laboratory (mFReal) at in Missouri University of Science and Technology. This combination enables the simultaneous capture of the bubble dynamics with the heat flux in the same vicinity. The local measurements by the probe were taken at seven dimensionless radial positions (r/R (-) = 0.0, ± 0.3, ± 0.6, ± 0.9) and in some cases nine positions, including ± 0.5. Since there was axis-symmetry, only results in one half (+r/R) have been reported. Three to five test runs were performed at each condition, and the average values were reported.

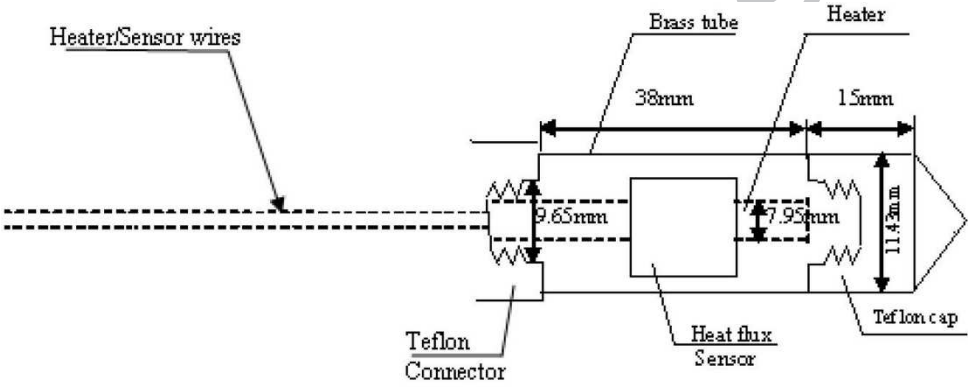

Figure 5. Heat transfer probe assembly: Schematic of the heat flux sensor and heater

According to Li and Prakash [33], to estimate the instantaneous heat flux and instantaneous heat transfer coefficients measured by the sensor, equation (12) has been employed, derived for liquid film heat transfer coefficients. From this equation, the instantaneous heat transfer coefficients could be determined by the measurement of heat flux per unit area and the difference between surface temperature and the average temperatures of the bulk fluid medium at a given time.

$$h_i = \frac{q_i}{T_{s_i} - T_{b_i}} \tag{12}$$

where h_i is the instantaneous local heat transfer coefficients, q_i is the instantaneous heat flux per unit area across the sensor, T_{b_i} is the instantaneous bulk temperature of the fluid media, and T_{s_i} is the instantaneous temperature of the probe surface. Likewise, the time-averaged heat transfer coefficients h_w was estimated at a given location by averaging the instantaneous heat transfer data collected after every 90s by equation (13):

$$h_w = \frac{1}{N}\sum_{i=1}^{N}\frac{q_i}{\left(T_{S_i} - T_{b_i}\right)} \tag{13}$$

2.3. Development of New Mechanistic Model for The Contact Time

In this section, the needed contact time, t_c, that properly represents the characteristic of the churn turbulent flow regime is developed, and the parameters related to it are examined. In this work, the distribution in the contact time, boundary layer estimation and heat transfer coefficients estimations using equation (4) is assessed by using the newly developed approach in estimating the contact time. In the measurements of the local gas hold-up, a number of studies have been done by fiber optical probes. Schweitzer et al. [42] used two point optical fibers to measure local gas hold-up in fluidized beds and slurry bubble columns, demonstrating that the optical probe spends different amount of time in the gas phase than it does in the liquid and pseudo-slurry phase. Detailed experimental studies [16], [35], [36] have shown that the optical probe stays different times in the liquid as it does in the gas bubbles. Moreover, the quantities of the heat transfer coefficients and bubble dynamics vary along the diameter or radial and the height of the column of gas-liquid or gas-liquid-solid (containment of the gas-liquid and gas-liquid-solid systems).

Accordingly, the local gas holdup is defined as a volume fraction occupied by the gas phase within a certain volume of interest within the mixture [38], [42] as shown in equation (14):

$$\varepsilon_{g,local} = \frac{V_{g,local}}{V_{g,local} + V_{l,local}} \tag{14}$$

This same definition can be extended to local gas hold-up for the pseudo-slurry mixture as well. By appealing the ergodic hypothesis, which states that "the ensemble average is equivalent to the time average," the spatially (volume) averaged local hold-up can be replaced by its equivalent time-averaged local hold-up, which is the ratio of the time bubbles passing through a unit volume to the sampling time. In the current study, the gas hold-up can be defined alternatively, like the time the probe tip spends in the gas bubbles to the sampling period. Thus, the local gas holdup could be expressed by equation (15):

$$\varepsilon_g = \frac{t_g}{t_g + t_l} \tag{15}$$

where ε_g, t_g, and t_l are the local gas hold-up, the time that the fiber probe tip spends in the bubble (gas phase) and the time that the probe spends in the liquid phase, respectively, during a sampling time τ. Over sampling time τ, N bubbles hit the fiber probe tip. The average time spent by the probe tip inside a bubble, $\bar{t_g}$, is given by equation (16):

$$\bar{t_g} = \frac{\varepsilon_g}{N}\tau \tag{16}$$

Similarly, the average time the probe spends in the liquid element $\bar{t}_l$ is shown in equation (17):

$$\bar{t}_l = \frac{\varepsilon_l}{\varepsilon_g}\bar{t}_g \tag{17}$$

where ε_l is the local liquid hold-up in equation (18)

$$\varepsilon_l = 1 - \varepsilon_g \tag{18}$$

Substituting Equations (16) and (18) into Equation (17) gives the contact time between the thin film and the liquid element as shown in equation (19):

$$\bar{t}_l = t_c = \left(1 - \varepsilon_g\right)\frac{\tau}{N} = \frac{\left(1 - \varepsilon_g\right)}{N/\tau} = \frac{\varepsilon_l}{N/\tau} \tag{19}$$

It is worth noting that τ/N is the inverse bubble pass frequency ν^{-1} over the optical probe fibers tip, and hence, over the heat transfer probe surface, since the optical probe tips are mounted just off the heat flux sensor. This approach indeed illustrates that the contact time is a function completely administrated by the local liquid holdup or local gas hold-up as $\varepsilon_l = \left(1 - \varepsilon_g\right)$ and bubble pass frequency. Consequently, the alteration of the heat transfer coefficients with the contact time occurs via the bubble pass frequency and the local phase hold-ups that are determined by the bubble velocity, bubble sizes and the gas-liquid specific interfacial area. It is therefore possible to obtain the mean local contact time by the hybrid measurements, local gas hold-up and local bubble pass frequency. Further, the bubble frequency can be misleading since it is an oversimplification for a highly poly-disperse bubbly flow. However, the four-point optical probe was validated in different flow regimes (bubbly, transition, and churn turbulent flow), in particular, using the sampling time equal to 138 (sec). Therefore, the effect of poly-disperse in the bubbly flow regime would be insignificant.

Using equations (9) for film thickness and (19) for contact time, the predicted heat transfer coefficients can be obtained via the mechanistic equation (4). It is also possible that rather than calculating only single values for the mean, a distribution of the heat transfer coefficients can also be obtained.

3. Results and Discussion

3.1. Contact Time

Figure 6 shows the radial profiles of the contact time, which is calculated by using equation (19), obtained from the measured bubble properties in the 18-inch diameter bubble column at different superficial gas velocities. As indicated in the above previous section, the contact time is estimated in this work from the bubble pass frequency and the local gas hold-up, both of which are interrelated to the bubble sizes and bubble velocity. From Figure 7, it can be seen that the contact time slope increases continuously towards the column wall, yielding much like parabolic profiles similar to the measured heat transfer coefficients and the reported bubble velocity, frequency, local hold-up, and specific interfacial area. This is an indication that the contact time determines the heat transfer rate as it depends on these bubble properties. Close to the wall, higher contact times are estimated due to lower bubble pass frequency and low gas hold-up. The low gas hold-up and low bubble pass frequency lead to a lower rate of the heat transfer surface renewal, which is an indication that bubble properties affect contact time that in turn affects the heat transfer coefficients.

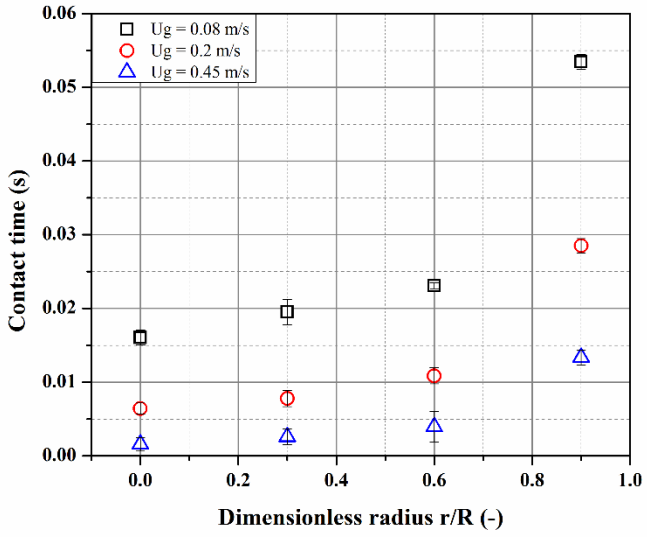

Figure 6. Effect of superficial gas velocity on the radial profiles of contact time in the 18-inch diameter bubble column

Figure 7 shows a comparison of the contact time for some of the reported methods in the literature. In this work, to obtain the contact time values predicted by the models of Li and Prakash [33] and Kumar and Fan [32], the length L of the heat flux sensor and the diameter of the heat transfer probe are utilized, while the bubble rise velocity measured by the four-point optical probe is used. As noted earlier on, at superficial gas velocities beyond 0.15 m/s, the bubble velocity does not change significantly. Thus, the two models give relatively close values to each other and remain nearly constant at 0.2 m/s or more. Since the length of the heat flux and probe diameter are fixed, the only determinant of the contact time becomes the bubble velocity. This represents a clear shortcoming of such an approach in estimating the contact time because the contact time is expected to vary (decrease) with increased superficial gas velocity, while the mixing and circulation are enhanced. On the other hand, the proposed model of this work predicts lower contact times at a higher range of superficial gas velocities than those of

the other two models [23], [33]. This difference can be attributed to the proposed model being able to capture the change in contact time due to enhanced mixing and recirculation along with bubble coalescence and breakage. A further increase in the local gas hold-up and bubble pass frequency with superficial gas velocity is also reflected. It should be noted that in the previous models, the bubble rise velocities of large bubbles were obtained by considering only the velocity of bubbles whose chord lengths are larger than the mean bubble chord length at a particular superficial gas velocity.

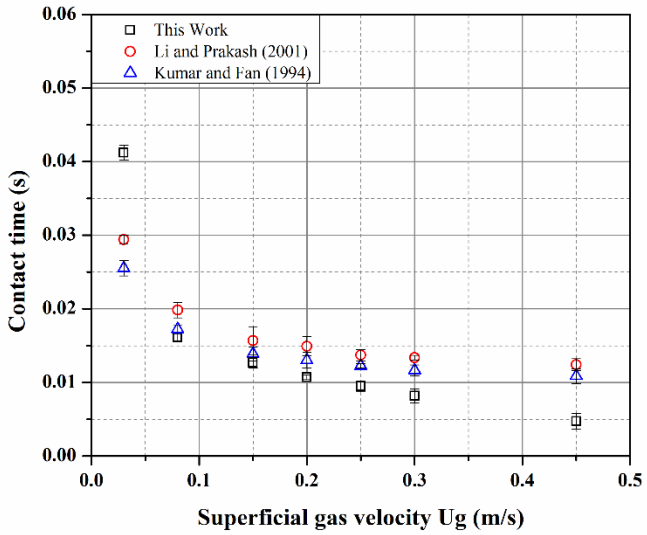

Figure 7. Contact time comparison with the reported models for the air-water system in the literature at the column center, r/R (-) = 0.0

The distribution of estimated contact time is illustrated in Figure 8 for an 18-inch bubble column at r/R (-) = 0 at two superficial gas velocities. The significantly small variances point to the fact that there is little spread in the local gas hold-up and bubble pass frequency at the point of measurements, and thus there is a narrow contact time distribution. However, relatively widespread contact time is observed at a higher superficial gas velocity. That is because, at a

higher superficial gas velocity, both the population of larger and smaller bubbles are produced relative to lower superficial gas velocity. Thus, it is expected that the heat transfer coefficients variation due to variation in contact time, has a wider spread at a higher superficial gas velocity. The proposed contact time model, equation (19), is simple but requires both the measurements of bubble pass frequency and local gas hold-up.

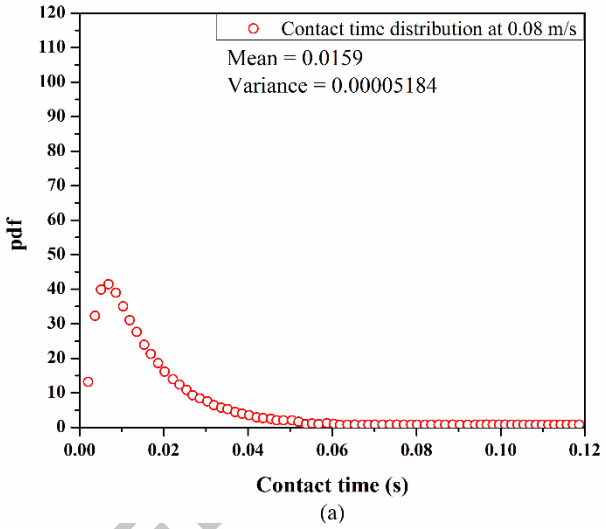

(a)

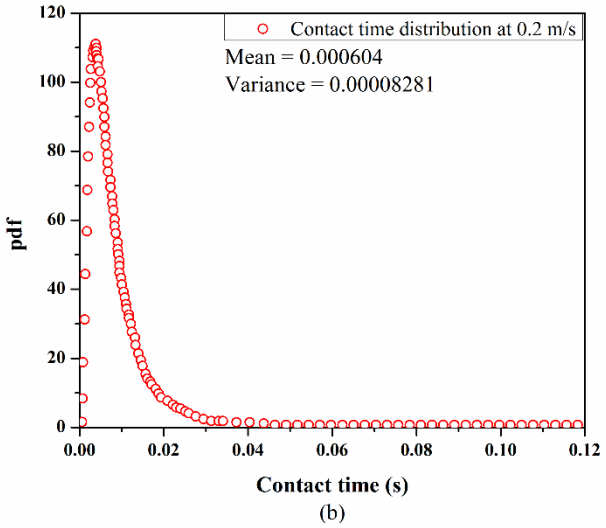

(b)

Figure 8. Distribution of the predicted contact time at r/R (-) = 0.0 (a) at U_g = 0.08 m/s (b) at U_g = 0.2 m/s

3.2. Film Thickness

Figure 9 illustrates the radial profiles of the estimated film thickness in the 18-inch bubble column using equation (9) and is based on the bubble properties measured by both measurement techniques. Even though the maximum film thickness is obtained close to the column wall just like the contact time with the minimum value at the column center, radial profiles are not necessarily similar. Increasing U_g from 0.08 m/s to 0.45 m/s leads to a decrease the film thickness by ~ 21 % and 9 % at the column center and wall region, respectively, with an average decrease of 15 %. At the lower superficial gas velocity (0.08 m/s), the wall region is also noted to have up to twice the film thickness at the column center and up to 2.4 times the film thickness at a higher superficial gas velocity U_g= 0.45 m/s. These variations can be attributed to a higher local axial bubble velocity and liquid velocity and hence more intensity of mixing, which gives rise to smaller values at the column center and at a higher superficial gas velocity.

Figure 10 shows a parity plot for film thickness that is evaluated by using equation (9) and other correlations as used in literature [22], [23], which were as follows in equation (20):

$$\delta = \frac{6.14\ L}{Re^{3/4} Pr^{1/3}} \tag{20}$$

They both defined Reynolds number and Prandtl's number, respectively, as $Re = U_b L \rho_l / \mu_l$ and $Pr = C_{pl} \mu_l / K_l$ with L being the vertical length of the heat transfer probe and U_b the bubble rise velocity. Kumar and Fan [32] used an equation similar to equation (20) in equation (21):

$$\delta = \frac{1.25\ d_p}{Re_p^{1/2} Pr^{1/3}} \tag{21}$$

where d_p is the probe diameter and Re_p is the Reynolds number based on the diameter of the probe with $U_{b,L}$ being the bubble rise velocity of large bubbles and defined as $Re_p = U_{b,L} d_p \rho_l / \mu_l$, with Prandtel's number defined as $Pr = C_{pl}\mu_l / K_l$. To obtain the bubble rise velocity of large bubbles, only the upward bubble velocity of the bubbles whose chord lengths were larger than the mean chord lengths were used. It is apparent that the differences between the predictions are due largely to the Reynolds numbers. The difference between the estimated film thickness and the correlations of Yang et al. [22], Li and Prakash [33], and Kumar and Fan [32] predictions are represented in terms of the average absolute relative difference (AARD) and the absolute relative difference (ARD), which are defined as follows in equations (22-23):

$$AARD = \frac{1}{N}\sum_{i=1}^{N}\left|\frac{\delta_{estimated} - \delta_{othercorr}}{\delta_{esrimated}}\right| \tag{22}$$

$$ARD = \left|\frac{\delta_{estimated} - \delta_{othercorr}}{\delta_{estimated}}\right| \tag{23}$$

It was determined that the film thickness that was predicted by other correlations [22], [23], [33] and those estimated in the current work, represented in equation (9), lie close to each other with an AARD of 15 %.

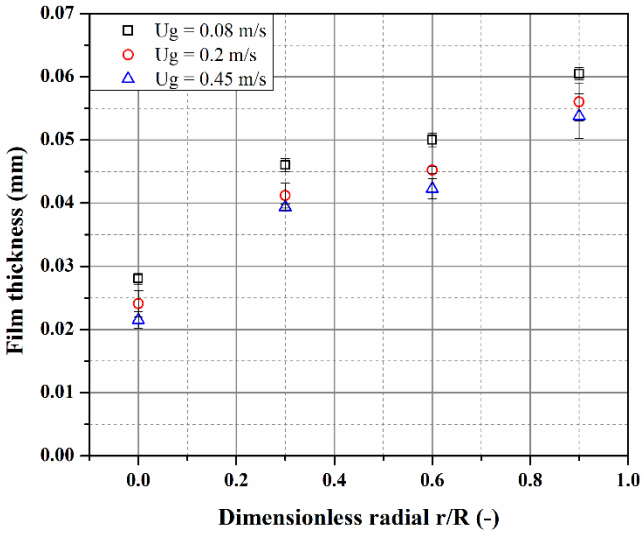

Figure 9. Effect of superficial gas velocity on radial profiles of estimated film thickness in an 18- inch bubble column

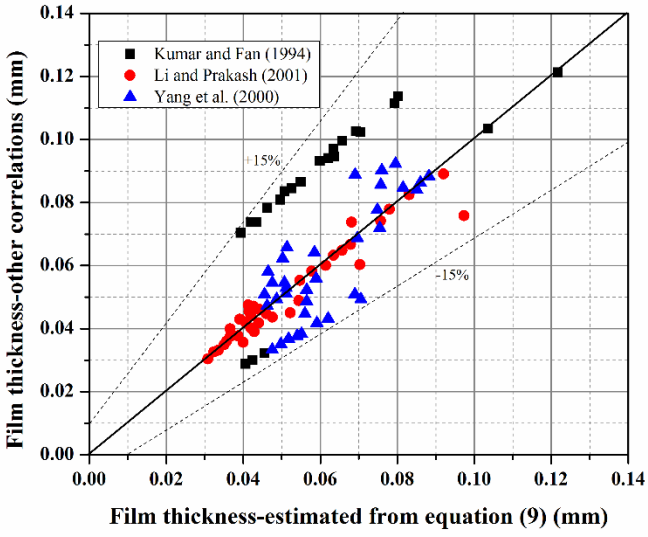

Figure 10. A parity plot of the estimated film thickness shown in equation (9) vs. film thickness estimated from correlations of Kumar and Fan (1994), Yang et al. (2001), and Li and Prakash (2001) in a bubble column

At any given superficial gas velocity, different sizes of bubbles are formed that move at different velocities. Hence, there is a distribution in the bubble velocities and bubble sizes, which are characterized by the bubble chord lengths. The distribution plots of the axial bubble velocity are provided elsewhere in Kagumba [19]. In equation (9), the Reynolds number is a function of both axial bubble velocity and bubble chord lengths, which have distributions. Thus, a distribution of estimated film thickness is obtained and shown in Figure 11. A near statistical similarity is observed in the distributions with little difference in variance. As expected, a smaller film thickness is obtained at U_g = 0.2 m/s than at U_g= 0.08 m/s.

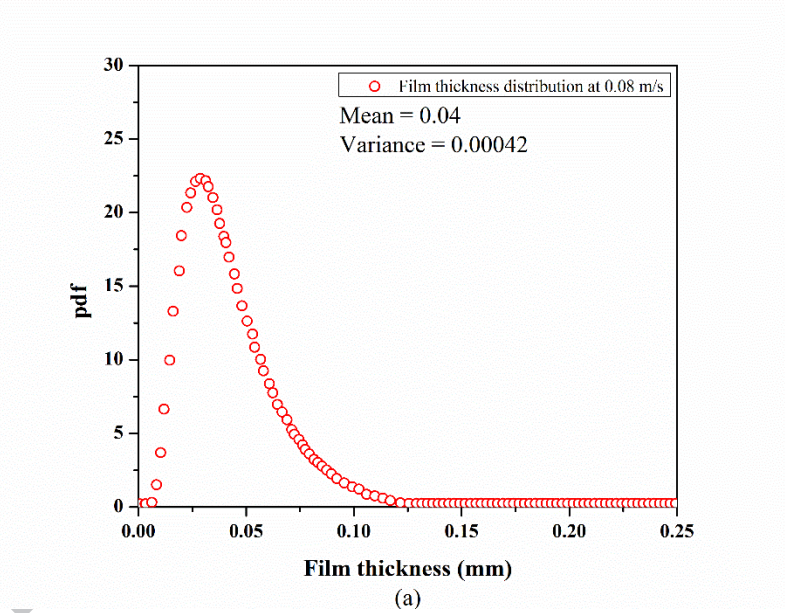

(a)

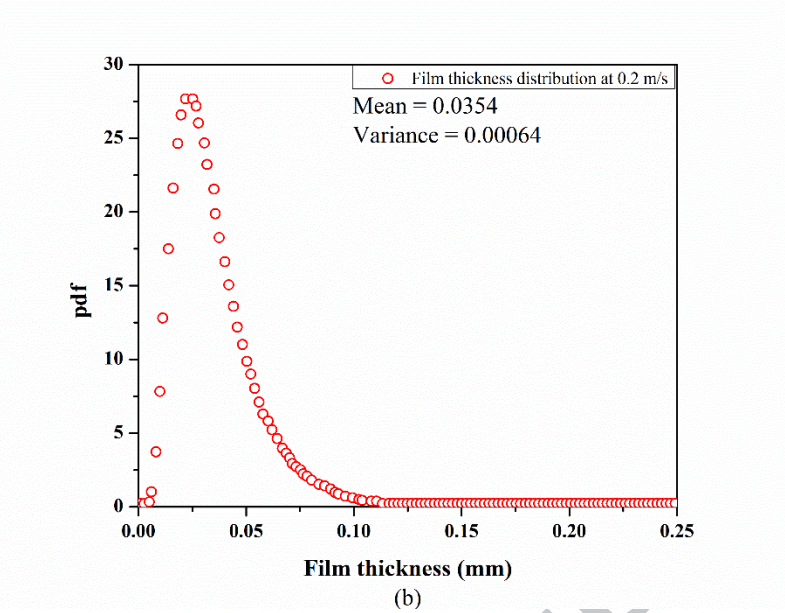

(b)

Figure 11. Distribution of the estimated boundary layer thickness in the 18-inch bubble column at r/R (-) = 0.0 (a) at U_g = 0.08 m/s (b) at U_g = 0.2 m/s

3.3. Heat Transfer Coefficients

The effect of superficial gas velocity on the radial profiles of the predicted heat transfer coefficients is presented in this section. Figure 12 compares the time-averaged instantaneous heat transfer data estimated by equation (4) at different radial locations from the center to the column wall for an air-water system for the superficial gas velocity U_g of 0.08 m/s, 0.2 m/s, and 0.45 m/s. It is observed that steepness of the radial profiles with superficial gas velocity increases from a low superficial gas velocity to a higher superficial gas velocity. For instance, at U_g = 0.08 m/s the radial profile has an average steepness of 1.2 towards the column wall, and this increases to 2.0 at U_g = 0.2 m/s and 2.4 at U_g = 0.45 m/s. Higher values are thus predicted at the center, which could be attributed to higher local turbulence generated by higher wake intensity due to, higher gas hold-up and bubble frequency, lower film thickness, and faster-moving bubbles in the central region of the column. Furthermore, it has been demonstrated that

large bubbles move towards the column center with higher velocity while smaller bubbles move closer to the wall region downwards at a lower velocity. It has also been demonstrated that the bubble pass frequency and gas hold-up are much higher at the column's center. This higher bubble frequency and hold up leads to shorter contact times and thinner films on the heat transfer surface thus enhancing the rate of renewal of the heat transfer surface.

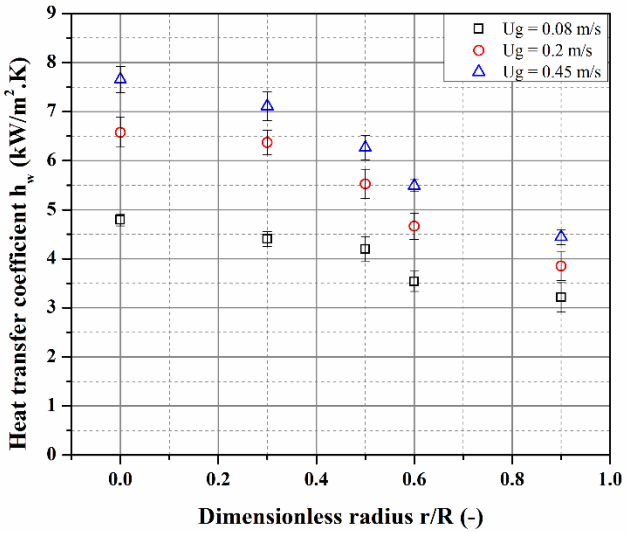

Figure 12. Effect of superficial gas velocity on radial profiles of predicted heat transfer coefficients in 18-inch bubble column

It is worth noting at this point that there are several studies reported in the literature about the parabolic profiles of the gas holding up as well as liquid velocity [41–46]. The parabolic shape of radial heat transfer profiles is generally similar to the radial profiles of gas hold-up and liquid velocity reported in literature studies, but it should be noted. However, that heat transfer is affected by both liquid velocity and turbulence generated by bubbles among other bubble properties. Hence, a direct comparison with gas hold-up, liquid velocity or any other bubble property profiles is not appropriate and may be misleading. However, the general trend

indicates that the wall region is relatively free of large bubbles or a faster moving chain of bubbles. Indeed, the measured bubble diameter is smaller near the wall region and larger in the center. The smaller diameter bubbles near the wall would have smaller wakes associated with them, resulting in a lower local heat transfer coefficients.

Figure 13 shows a comparison between the mean predicted heat transfer coefficients, modeled in equation (4), and the heat transfer coefficients that is measured. The predicted heat transfer coefficients were obtained based on the bubble properties measured at the same time as the measurements of the heat transfer coefficients using a fast response heat transfer probe. At 0.08 m/s, the predicted heat transfer coefficients shown in Figure 13 are 7.3 % and 6.1 % higher than measured at the column center region ($r/R \leq 0.3$) and at the column wall region ($r/R \geq 0.6$), respectively. These differences increase further with superficial gas velocity. At 0.45 m/s, an increase of 11.3 % and 9 % is noted. At the column center and higher superficial gas velocity, much shorter contact times are estimated by the new model. At such short contact times, shorter than the response time of the heat flux probe, the heat transfer wake-enhanced phenomenon cannot be captured by the heat transfer probe. At the column wall region, relatively longer contact times are estimated. Nevertheless, the estimated heat transfer coefficients still falls within 12 % of the measured coefficients.

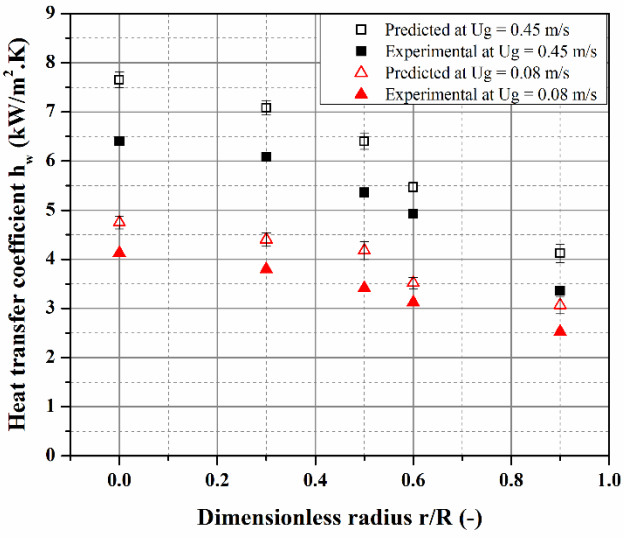

Figure 13. Comparison of the predicted heat transfer coefficients shown in equation (4) with the measured heat transfer coefficients values in an 18-inch bubble column

Figure 14 shows the predictions of the proposed model compared against the experimental data of the measured heat transfer coefficients using the fast response heat transfer probe developed and utilized in this work for a wide range of operating conditions. The necessary model parameters are obtained from the hybrid technique measurement results. Figure 14 demonstrates that the model over-predicts the heat transfer coefficients and this would be due to the estimation of the film thickness and the contact time and how the contact time would impact the actual values of the film thickness. Thus, sensitivity analysis is recommended to quantify such impact. However, to further assess the performance of the correlation model predictions statistically, the average absolute relative error (AARE) has been used and is calculated as follows in equation (24):

$$AARE = \frac{1}{N}\sum_{i=1}^{N}\left|\frac{h_{w,predicted} - h_{w,experimental}}{h_{w,experimental}}\right| \quad (24)$$

A very good agreement, within 13 %, was found between the predicted and the experimental values of the heat transfer coefficients, even though the model overpredicts the heat transfer coefficients at all the evaluated conditions. One of the main reasons why the proposed model overpredicts the heat transfer coefficients is that the new approach of estimating the contact time, as shown in equation (19), predicts up to very low values of contact time. In fact, at 0.2 m/s in an 18-inch column, the estimated contact time is 0.006, which is almost an order of magnitude less than the response time of the heat flux and temperature sensor.

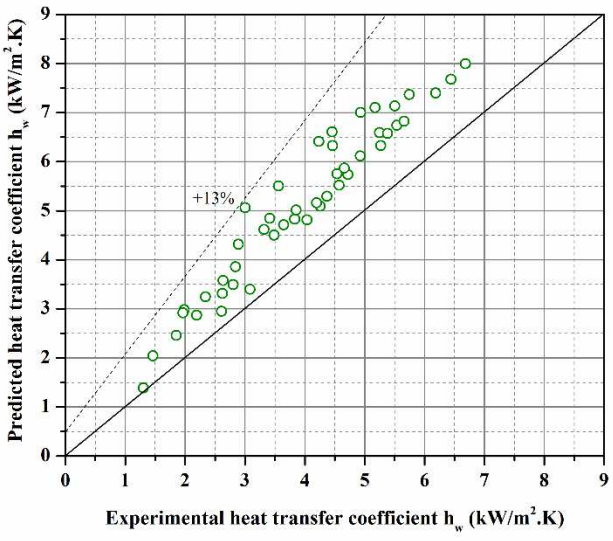

Figure 14. A parity plot of the predicted heat transfer coefficients by equation (4) vs. the measured heat transfer coefficients values in the bubble columns at the same operating conditions

3.4. Heat Transfer Coefficients and Bubble Dynamics Distribution

The reported heat transfer coefficients in the open literature shows the average values only. However, in an industrial system at the same superficial gas flow rate, the values vary significantly over time. With distributions in the measured bubble properties as well as in both

the contact time and film thickness, it is, therefore, possible that a distribution of the predicted heat transfer coefficients can be obtained. The simulated distribution was extracted from experimental data collected for 90 seconds. In Figure 15 (a and b) it is demonstrated that there is distribution of the heat transfer coefficients both at 0.08 m/s and at 0.2 m/s, respectively. In fact, a wider distribution in the heat transfer coefficients is reported at a higher superficial gas velocity than at a lower superficial gas velocity.

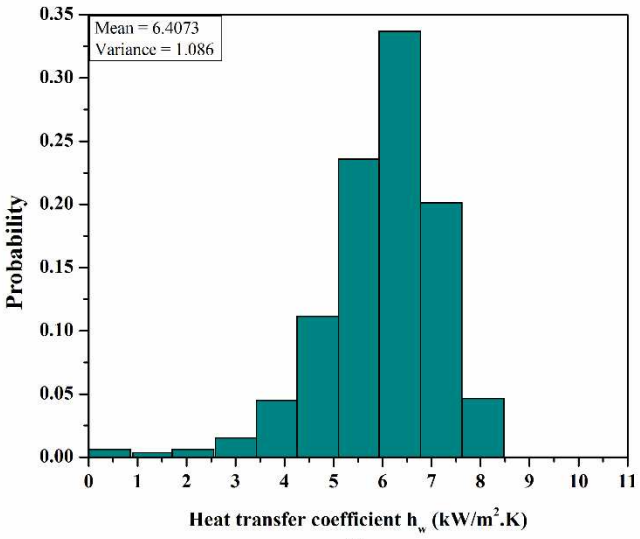

(a)

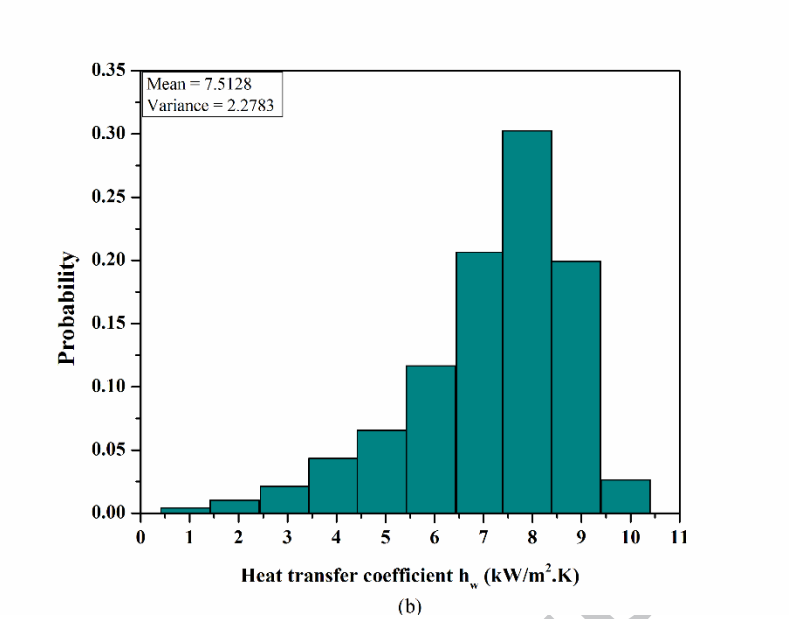

Figure 15. Histogram of the probability distribution of predicted heat transfer coefficients at r/R (-) = 0.0 (a) U_g = 0.08 m/s (b) U_g = 0.2 m/s

Figure 16 (a-b) and Figure 17 (a-b) show the histogram for the probability density function (pdf) distribution of bubble chord lengths and axial bubble velocity, respectively, at 0.08 m/s and 0.2 m/s. At a higher superficial gas velocity, there is growth in the population of both large and small bubbles, hence a wider spread of the bubble sizes (chord lengths). The different sizes of bubbles move at different velocities that create different intensities of the heat transfer surface renewal rate. It should also be pointed out that some of the smaller bubbles are entrained and dragged in the wake of larger ones and move at nearly the same velocity as that of the large bubbles. The mean of the distribution of the heat transfer coefficients was found to be 1.8 % and 3.1 % higher than the predicted average at U_g = 0.08 m/s and 0.2 m/s, respectively.

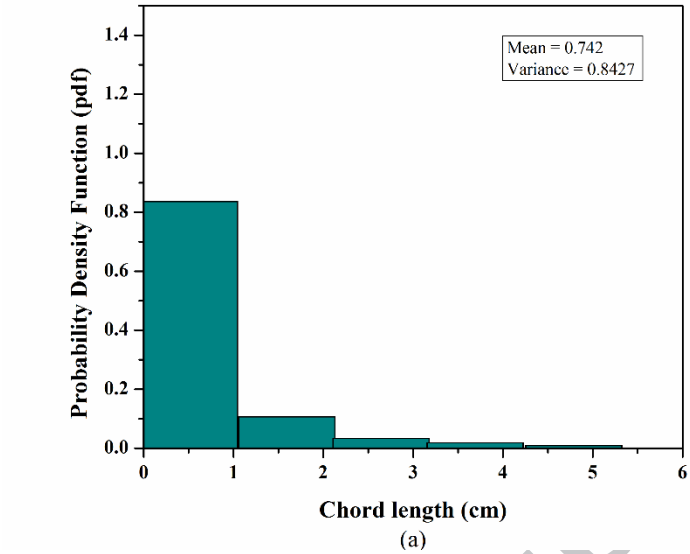

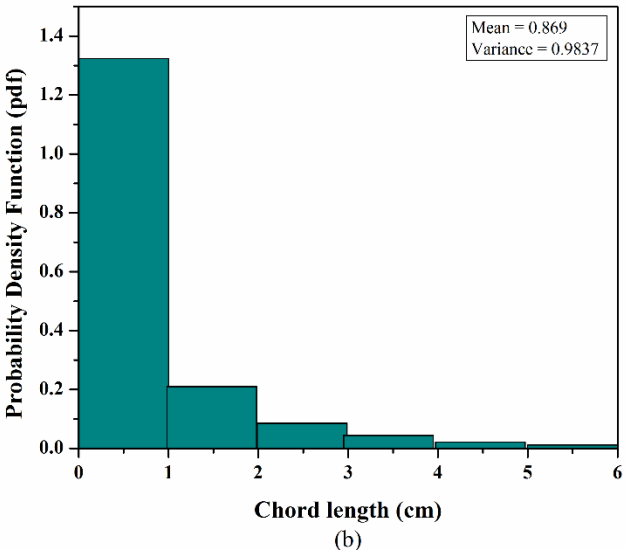

Figure 16. Histogram of the probability density function (pdf) distribution of bubble chord lengths r/R (-) = 0.0(a) U_g = 0.08 m/s (b) U_g = 0.2 m/s

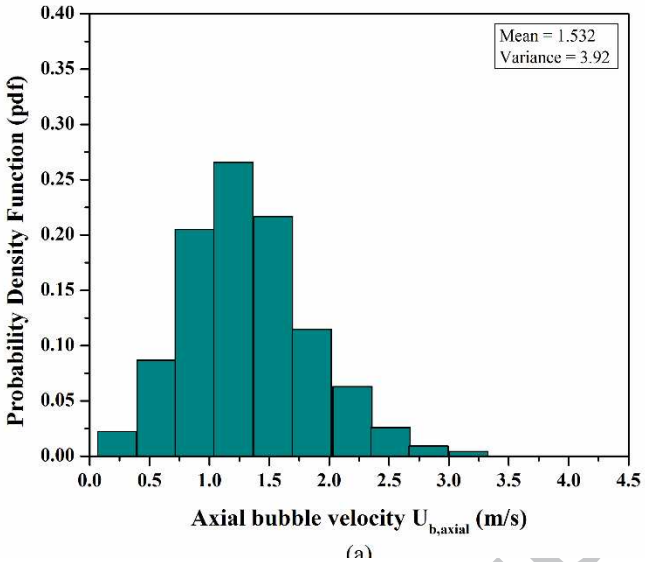

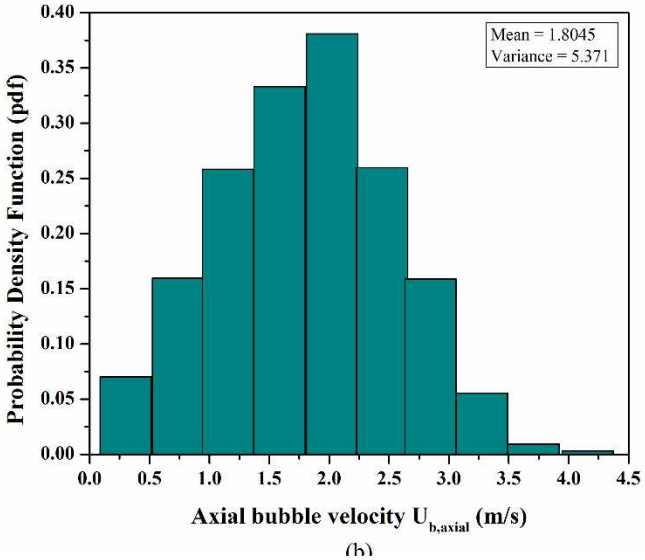

Figure 17. Histogram of the probability density function (pdf) distribution of the axial bubble at r/R (-) = 0.0 (a) U_g = 0.08 m/s (b) U_g= 0.2 m/s.

4. Conclusions

1. For the first time, a combined probe, which consists of a fast-response heat transfer coefficients probe and an advanced four-point optical probe, was used for simultaneously measuring the heat transfer coefficients and the bubble properties, respectively, to develop a new mechanistic model has been proposed based on local bubble properties and has been used to estimate the contact time needed for the mechanistic model of heat transfer coefficients prediction and successfully implemented in the estimation of heat transfer.
2. The mechanistic analysis shows that the contact time between the thin film and the liquid element is a function of the local phase hold-up and bubble pass frequency, all of which are dependent on other bubble properties such as the specific interfacial area, bubble sizes, and bubble velocity.
3. The heat transfer coefficients significantly depended on both the distribution of bubble velocity and the bubble properties, including local gas holdup and bubble frequency on the heating surface.

4. The variation of the local time-averaged heat transfer coefficients with the contact time occurs via the bubble pass frequency and the local phase hold-ups. Hence, it has been shown that with a proper model of the contact time estimation, the mechanistic model of the heat transfer coefficients that is obtained using a continuous film and unsteady state surface renewal mechanistic approach can accurately predict the heat transfer coefficients without fitting parameters from the solid surface (probe surface) to the flowing gas and liquid.
5. The proposed model could be implemented by the numerical methods, particularly, CFD simulation to calculate the heat transfer coefficients as well as by coupling the proposed model with the population balance model (PBM).

Acknowledgments

The authors gratefully acknowledge the financial assistance provided by Multiphase Flow and Multiphase Reactor Engineering and Application Laboratory (mFReal) to develop the four-point optical fiber probe technique, the Chemical and Biochemical Engineering Department at Missouri University of Science and Technology and the Higher Committee for Education Development in Iraq (HCED), which made this work possible.

Nomenclature

(AARD) = Average absolute relative difference

(ARD) = Absolute relative difference

$U_{b,axial}$ = Axial bubble velocity (cm/s)

$U_{b,L}$ = Rise velocity of large bubble (cm/s)

U_b = Bubble rise velocity (cm/s)

U_g = Superficial gas velocity (m/s)

$V_{g,local}$ = Local gas phase volume (cm^3)

$V_{l,local}$ = Local liquid phase volume (cm^3)

N = Total number of bubbles (riser and comedown) in equations 16 and 19, and a number of sample in equations 13, 22, and 24.

$\varepsilon_g, \varepsilon_{g,local}$ = Local gas holdup (volume fraction)

L = Vertical length of heat sensor (m)

T_w = Wall temperature (K)

T_0 , T_y = Bulk temperature (K)

T_{bi} = Instantaneous bulk temperature (K)

T_{si} = Instantaneous temperature of the probe surface (K)

q_i = Instantaneous heat flux per unit area

t_c, θ_c = Contact time (sec)

t_g = The time that the fiber probe tip spends in one bubble (sec)

$\overline{t_g}$ = Average time that the fiber probe tip spends in gas phase (bubble) (sec)

t_l = the time that the fiber probe tip spends in liquid phase (sec)

$\overline{t_l}$ = Average time that the fiber probe tip spends in liquid phase (sec)

τ = Total sampling time (sec)

h_i = Instantaneous heat transfer coefficients (kW/m^2.K)

h = Heat transfer coefficients (kW/m^2.K)

h_w = Average heat transfer coefficients (kW/m^2.K)

l_c = Bubble chord length (m)

ρ_l = Liquid density (kg/m^3)

ρ = Liquid density (kg/m^3)

K_l = Liquid thermal conductivity (W/m.K)

μ_l = Liquid viscosity (cp)

C_{pl} = Specific heat capacity of the liquid (J/kg.K)

k = Thermal conductivity (W/m.K)

α = Thermal diffusivity of the liquid and slurry (cm^2/s)

s = Fraction rate of surface renewal

d_p = Heat transfer probe diameter (m)

ν = Liquid kinematic viscosity (cm^2/s)

δ_0 = Laminar viscous sublayer (m)

δ = Thermal boundary layer (m)

δ_e = Uniform film thickness (m)

Re = Reynolds number ($U_b L \rho_l / \mu_l$)

Re_p = Reynolds number $\left(U_{b,L} d_p \rho_l / \mu_l\right)$

Pr = Prandtl number $\left(C_{pl} \mu_l / K_l\right)$

θ = Time duration (sec)

i = Time series (sec)

PBM = Population Balance Model

References

[1] C. Maretto and R. Krishna, "Modelling of a bubble column slurry reactor for Fischer-Tropsch synthesis," *Catal. Today*, vol. 52, no. 2–3, pp. 279–289, 1999.

[2] W. -D. Deckwer and E. Alper, "Katalytische Suspensions-Reaktoren," *Chemie Ing. Tech.*, vol. 52, no. 3, pp. 219–228, 1980.

[3] Y. Kato, K. Uchida, T. Kago, and S. Morooka, "Liquid holdup and heat transfer coefficients between bed and wall in liquid solid and gas-liquid-solid fluidized beds," *Powder Technol.*, vol. 28, no. 2, pp. 173–179, 1981.

[4] T. -M. Chiu and E. N. Ziegler, "Heat transfer in three-phase fluidized beds," *AIChE J.*, vol. 29, no. 4, pp. 677–685, 1983.

[5] Y. Kang, I. S. Suh, and S. D. Kim, "Heat Transfer Characteristics of Three Phase Fluidized Beds," *Chem. Eng. Commun.*, vol. 34, no. 1–6, pp. 1–13, 1985.

[6] S. D. Kim, Y. Kang, and H. K. Kwon, "Heat transfer characteristics in two- and three-phase slurry-fluidized beds," *AIChE J.*, vol. 32, no. 8, pp. 1397–1400, 1986.

[7] M. Magiliotou, Y. -M. Chen, and L. -S. Fan, "Bed-immersed object heat transfer in a three-phase fluidized bed," *AIChE J.*, vol. 34, no. 6, pp. 1043–1047, 1988.

[8] S. C. Saxena, N. S. Rao, and A. C. Saxena, "Heat-transfer and gas-holdup studies in a bubble column: air-water-glass bead system," *Chem. Eng. Commun.*, vol. 96, no. 1, pp. 31–55, 1990.

[9] S. C. Saxena, N. S. Rao, and A. C. Saxena, "Heat transfer from a cylindrical probe immersed in a three-phase slurry bubble column," *Chem. Eng. J.*, vol. 44, no. 3, pp. 141–

156, 1990.

[10] S. C. Saxena, N. S. Rao, and A. C. Saxena, "Heat transfer and gas holdup studies in a bubble column: Air-water-sand system," *Can. J. Chem. Eng.*, vol. 70, no. 1, pp. 33–41, 1992.

[11] N. Kantarci, K. O. Ulgen, and F. Borak, "A study on hydrodynamics and heat transfer in a bubble column reactor with yeast and bacterial cell suspensions," *Can. J. Chem. Eng.*, vol. 83, no. 4, pp. 764–773, 2005.

[12] F. . Campos and P. L. . Lage, "Heat and mass transfer modeling during the formation and ascension of superheated bubbles," *Int. J. Heat Mass Transf.*, vol. 43, no. 16, pp. 2883–2894, 2000.

[13] D. Colombet, E. Goncalvès Da Silva, and R. Fortes-Patella, "On numerical simulation of cavitating flows under thermal regime," *Int. J. Heat Mass Transf.*, vol. 105, pp. 411–428, 2017.

[14] C. Dang, L. Jia, Q. Peng, Q. Huang, and X. Zhang, "Experimental and analytical study on nucleate pool boiling heat transfer of R134a/R245fa zeotropic mixtures," *Int. J. Heat Mass Transf.*, vol. 119, pp. 508–522, 2018.

[15] K. Kaiho, T. Okawa, and K. Enoki, "Measurement of the maximum bubble size distribution in water subcooled flow boiling at low pressure," *Int. J. Heat Mass Transf.*, vol. 108, pp. 2365–2380, 2017.

[16] C. Wu, "Heat Transfer and Bubble Dynamics in Slurry Bubble Columns for Fischer-Tropsch Clean Alternative energy," Washington University, 2007.

[17] S. Kumar, K. Kusakabe, K. Raghunathan, and L. -S. Fan, "Mechanism of heat transfer in bubbly liquid and liquid-solid systems: Single bubble injection," *AIChE J.*, vol. 38, no. 5, pp. 733–741, 1992.

[18] M. Kagumba and M. H. Al-Dahhan, "Impact of internals size and configuration on bubble dynamics in bubble columns for alternative clean fuels production," *Ind. Eng. Chem. Res.*, vol. 54, no. 4, pp. 1359–1372, 2015.

[19] M. Kagumba, "Heat transfer and bubble dynamics in bubble and slurry bubble columns with internals for Fischer-Tropsch synthesis of clean alternative fuels and chemicals," Missouri University of Science and Technology, 2013.

[20] A. K. Jhawar and A. Prakash, "Heat Transfer in a Slurry Bubble Column Reactor: A Critical Overview," *Ind. Eng. Chem. Res.*, vol. 51, no. 4, pp. 1464–1473, 2012.

[21] D. T. Wasan and M. S. Ahluwalia, "Consecutive film and surface renewal mechanism for heat or mass transfer from a wall," *Chem. Eng. Sci.*, vol. 24, no. 10, pp. 1535–1542, 1969.

[22] G. Q. G. Yang, X. Luo, R. Lau, and L. S. Fan, "Heat-Transfer Characteristics in Slurry Bubble Columns at Elevated Pressures and Temperatures," *Ind. Eng. Chem. Res.*, vol. 39, no. 7, pp. 2568–2577, 2000.

[23] S. Kumar and L. -S.-S. Fan, "Heat-transfer characteristics in viscous gas-liquid-solid systems," *AIChE J.*, vol. 40, no. 5, pp. 745–755, 1994.

[24] W. Nernst, "Theorie der Reaktionsgeschwindigkeit in heterogenen Systemen," *Zeitschrift für Phys. Chemie*, vol. 47, no. 1, pp. 52–55, 1904.

[25] D. Azbel, *Two-phase flows in chemical engineering*. Cambridge Univeristy Press, 1981.

[26] Ralph Higbie, "The rate of absorption of a pure gas into still liquid during short periods of exposure," *Trans. IChmE*, vol. 31, no. 2, pp. 365–389, 1935.

[27] P. V. Danckwerts, "Significance of Liquid-Film Coefficients in Gas Absorption," *Ind. Eng. Chem.*, vol. 43, no. 6, pp. 1460–1467, 1951.

[28] M. G. Cooper, "The microlayer and bubble growth in nucleate pool boiling," *Int. J. Heat Mass Transf.*, vol. 12, no. 8, pp. 915–933, Aug. 1969.

[29] K. Moriyama and A. Inoue, "Thickness of the Liquid Film Formed by a Growing Bubble in a Narrow Gap Between Two Horizontal Plates," *J. Heat Transfer*, vol. 118, no. 1, pp. 132–139, 1996.

[30] T. A. Shedd and T. A. Newell, "Characteristics of the liquid film and pressure drop in horizontal, annular, two-phase flow through round, square and triangular tubes," *J. Fluids Eng. Trans. ASME*, vol. 126, no. 5, pp. 807–817, 2004.

[31] H. Li and a. Prakash, "Heat Transfer and Hydrodynamics in a Three-Phase Slurry Bubble Column," *Ind. Eng. Chem. Res.*, vol. 36, pp. 4688–4694, 1997.

[32] S. Kumar and L. -S. Fan, "Heat-transfer characteristics in viscous gas-liquid and gas-liquid-solid systems," *AIChE J.*, vol. 40, no. 5, pp. 745–755, 1994.

[33] H. Li and A. Prakash, "Survey of heat transfer mechanisms in a slurry bubble column," *Can. J. Chem. Eng.*, vol. 79, no. 5, pp. 717–725, 2001.

[34] H. Schlichting, *Boundary Layer Theory*, 8th ed. Springer, 2017.

[35] J. Xue, M. Al-Dahhan, and M. P. Dudukovic, "Bubble Velocity, Size, and Interfacial Area Measurements in a Bubble Column by Four-Point Optical Probe," *AIChE J.*, vol. 54, no.

2, pp. 350–363, 2008.

[36] A. A. Youssef and M. H. Al-Dahhan, “Impact of internals on the gas holdup and bubble properties of a bubble column,” *Ind. Eng. Chem. Res.*, vol. 48, no. 17, pp. 8007–8013, 2009.

[37] J. J. Frijlink, “Physical aspects of gassed suspension reactors,” Delft University of Technology, 1987.

[38] J. Xue, “Bubble Velocity , Size and Interfacial Area Measurements in Bubble Columns,” Washington Univeristy, Saint Louis, 2004.

[39] J. Xue, M. Al-Dahhan, M. P. Dudukovic, and R. F. Mudde, “Four-point optical probe for measurement of bubble dynamics: Validation of the technique,” *Flow Meas. Instrum.*, vol. 19, no. 5, pp. 293–300, 2008.

[40] A. Youssef, “Fluid Dynamics and Scale-up of Bubble Columns with Internals,” Washington University in St. Louis, 2010.

[41] R. S. Abdulmohsin and M. H. Al-Dahhan, “Impact of internals on the heat-transfer coefficients in a bubble column,” *Ind. Eng. Chem. Res.*, vol. 51, no. 7, pp. 2874–2881, 2012.

[42] J.-M. Schweitzer, J. Bayle, and T. Gauthier, “Local Gas Hold-Up Measuments in Fluidized Bed and Slurry Bubble Column,” *Chem. Eng. Sci.*, vol. 56, pp. 1103–1110, 2001.

[43] J. H. Hills, “Radial Non-Uniformity of Velocity and Voidage in a Bubble Column,” *Trans. Inst. Chem. Eng.*, vol. 52, pp. 1–9, 1974.

[44] K. Ueyama, S. Morooka, K. Kolde, H. Kaji, and T. Mlyauchi, "Behavior of Gas Bubbles in Bubble Columns," *Ind. Eng. Chem. Process Des. Dev.*, vol. 19, no. 4, pp. 592–599, 1980.

[45] R. Nottenkaemper, A. Steiff, and P.-M. Weinspach, "Experimental Investigation of Hydrodynamics of Bubble Columns," *Ger. Chem. Eng.*, vol. 6, no. 3, pp. 147–155, 1983.

[46] Y. Wu and M. H. Al-Dahhan, "Prediction of axial liquid velocity profile in bubble columns," *Chem. Eng. Sci.*, vol. 56, no. 3, pp. 1127–1130, 2001.

[47] H. Luo and H. F. Svendsen, "Turbulent Circulation in Bubble Column from Eddy Viscosity Distributions of Single-Phase Flow," *Can. J. Chem. Eng.*, vol. 69, no. 6, pp. 1389–1394, 1991.

[48] A. Shaikh, "Bubble and slurry bubble column reactors: Mixing, flow regime transition and scaleup," *PhD Diss. Washingt. Univ. St. Louis,* no. August, p. 281, 2007.

To,

The Editor

Chemical Engineering Journal

From,

Muthanna Al-Dahhan (*aldahhanm@mst.edu*)

Missouri University of Science and Technology
Chemical and Biochemical Engineering Department
110E, Bertelsmeyer Hall, Rolla, MO 65409 USA
Phone: +1 (573) 341 7518

Manuscript title: A New Contact Time Model for Mechanistic Assessment of Local Heat Transfer Coefficients in Bubble Column Using Both Simultaneously Four-Optical Fiber Probe and Fast Heat Transfer Probe.

Highlights

- Bubble pass frequency and local gas holdup impact the contact time
- The bubble properties affect the magnitude of the heat transfer coefficient
- Work provides a new model to calculate heat transfer coefficient by CFD simulation